ACS OMEGA

Open Access

http://pubs.acs.org/journal/acsodf

Article

Dynamic Oligomerization Processes of *Bacillus subtilis* ClpP Protease Induced by ADEP1 Studied with High-Speed Atomic Force Microscopy

Fumihiro Ishikawa,*[,#] Kanji Takahashi,[#] Akiko Takaya, Genzoh Tanabe,* Michio Homma, and Takayuki Uchihashi*

Cite This: *ACS Omega* 2025, 10, 7381−7388

Read Online

ACCESS | Metrics & More | Article Recommendations | Supporting Information

ABSTRACT: Bacterial ClpPs are a highly conserved family of serine proteases that associate with members of the AAA+ ATPase (ATPase associated with diverse cellular activities) family to degrade protein substrates. The antibiotic A54556 factor (ADEP1) induces uncontrolled proteolysis by forming an ATPase-independent ClpP-ADEP complex. Cryo-EM analysis of *Bacillus subtilis* ClpP (*Bs*-ClpP) has demonstrated that ADEP1 binding shifts the protease to an active extended conformation and opens its axial entry pores. However, the dynamic oligomerization processes of *Bs*-ClpP induced by ADEP1 remain unclear. In this study, we used a combination of biochemical studies and high-speed atomic force microscopy (HS-AFM) to reveal how ADEP1 affects the oligomerization states and protease activity of *Bs*-ClpP, inducing the active extended state and protease activity of *Bs*-ClpP. HS-AFM observations demonstrated that the *Bs*-ClpP tetradecamer (2R state) forms via a progression from monomers to oligomers and then from oligomers to heptamers (R state) in the presence of ADEP1. Our results suggest that ADEP1 binding to monomeric *Bs*-ClpP triggers conformational changes that facilitate *Bs*-ClpP oligomerization (R and 2R states) and activation.

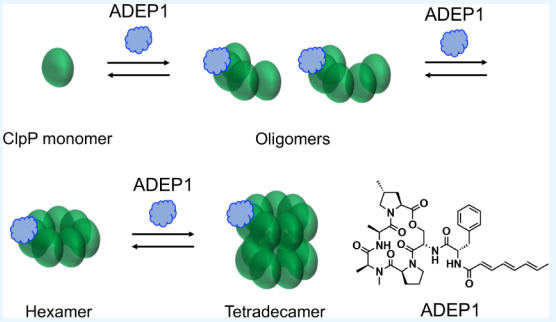

INTRODUCTION

Protein homeostasis, maintained through a balance of synthesis and degradation, is crucial for all living organisms. While synthesis is primarily regulated at the transcriptional and translational levels, degradation is carried out by various proteases with specific activation mechanisms. The Clp (Chaperonin-linked-protease) complex, a key proteolytic system present in prokaryotic and eukaryotic cell organelles (such as mitochondria), plays a significant role in this process. This complex is composed of the serine protease ClpP and AAA+ ATPase (ATPases associated with diverse cellular activities), including ClpX or ClpC.[1−4] The Clp proteolytic complex is a tetradecamer structure formed by the stacking of two heptameric rings of ClpP. A hexameric ring of ATPase, such as ClpX or ClpC attaches to one or both sides of this tetradecameric ClpP structure. The current understanding is that the ATPase complex selectively unfolds specific proteins and translocates them into the ClpP complex for degradation. Importantly, ClpP alone is unable to degrade the proteins *in vivo*, highlighting the essential role of the ATPase component in this process.[5,6]

A54556 factor A (ADEP1) isolated from *Streptomyces hawaiiensis* NRRL 15010 (Figure 1A) has garnered attention as a potential antibiotic due to its ability to target ClpP and exhibit antibacterial activity.[7,8] ClpP is a highly conserved protein across various animal and bacterial species (Figure S1). This high degree of homology has led to the development of ADEP1 derivatives not only as antibiotics but also as potential cancer therapeutics that modulate mitochondrial functions in humans.[9,10] ADEP1 and its analogues, which are hydrophobic molecules, bind to ClpP in a hydrophobic pocket located at the interface between ClpP monomers.[11] This binding activates the ClpP protease independently of ClpX. ADEP1 inhibits bacterial growth by inducing a conformational change in ClpP that enlarges its central ring pore, which serves as the entry point for substrate proteins (Figure S2).[12,13] It has been speculated from the crystal structures that the distinctive barrel conformations, called compressed, compact, or extended state are taken during the reaction.[14−16] Previous studies have demonstrated that ClpP from *Bacillus subtilis* (*Bs*-ClpP) is purified in monomeric form in the absence of glycerol. The addition of either glycerol or ADEP1 rapidly induces the

Received: December 15, 2024
Revised: January 27, 2025
Accepted: January 31, 2025
Published: February 12, 2025

https://doi.org/10.1021/acsomega.4c11303
ACS Omega 2025, 10, 7381−7388

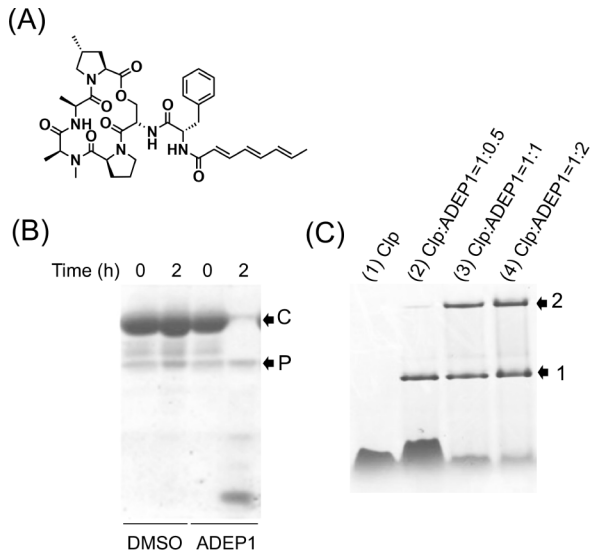

Figure 1. Detection of *Bs*-ClpP oligomerization and protease activity. (A) Structure of A54556 factor A (ADEP1). (B) Casein degradation assay. A mixture of *Bs*-ClpP and casein with DMSO (control) or ADEP1 was incubated for 0 or 2 h at 37 °C. The proteins in the mixture were separated using a SDS-PAGE gel and detected by CBB staining. Arrow C indicates casein, and arrow P indicates ClpP. (C) Native-PAGE analysis of the *Bs*-ClpP oligomerization. A mixture of *Bs*-ClpP with DMSO (control) or ADEP1 was incubated for 30 min at 37 °C. ADEP1 was mixed at a monomer molar ratio of *Bs*-ClpP:ADEP1 = 1:0.5, 1:1, or 1:2. The proteins in the mixture were separated by Native-PAGE and detected by CBB staining. High molecular weight bands (1) and (2) with slow mobility were detected, indicating the formation of higher-order oligomers.

formation of tetradecameric complexes.[17−19] However, it is important to note that while both glycerol and ADEP1 promote oligomerization, only the ADEP1-induced tetradecameric complex exhibits protease activity. The glycerol-induced tetradecamer remains proteolytically inactive, highlighting the specific activating effect of ADEP1 on *Bs*-ClpP.

Understanding how ADEP1 affects the structure of ClpP and how these conformational changes relate to protease activity is crucial for drug discovery and development. Particularly, the dynamic oligomerization processes of *Bs*-ClpP induced by ADEP1 have remained unclear. In this study, we employed high-speed atomic force microscopy (HS-AFM) as our primary investigative tool to analyze how ADEP1 influences the oligomerization states of ClpP. This approach allows us to directly observe and characterize the dynamic assembly processes of *Bs*-ClpP in response to ADEP1 binding, providing insights into the mechanism of ADEP1-induced ClpP activation at the molecular level.

RESULTS

Purification of *Bs*-ClpP and Detection of Protease Activity. The *B. subtilis clpP* gene, cloned into a pET vector with an added C-terminal six-residue histidine affinity tag (His-tag), was expressed in *E. coli* and subsequently purified using His-tag affinity chromatography (Figure S3). The protease activity of purified *Bs*-ClpP was assessed using a casein degradation assay (Figure 1A). In the absence of ADEP1, purified *Bs*-ClpP alone showed no detectable casein degradation. However, upon the addition of ADEP1, significant casein degradation was observed, confirming the ADEP1-dependent activation of *Bs*-ClpP's proteolytic activity.

Multimer formation of *Bs*-ClpP induced by ADEP1 was analyzed using native gel electrophoresis (Figure 1B). In the presence of ADEP1, two distinct high-molecular-weight bands (band 1 and band 2) with low mobility were observed, which were absent in samples without ADEP1. The intensity of these high-molecular-weight bands increased proportionally with the ADEP1 to *Bs*-ClpP molar ratio. Based on their molecular weights, band 2 at the high-molecular-weight position is presumed to correspond to the tetradecameric form *Bs*-ClpP, while band 1 at the low-molecular-weight position likely represents the heptameric form. In the absence of ADEP1, a smeared band was observed and probably corresponds to various oligomeric states of ClpP. These results confirm that ADEP1 promotes the formation of specific higher-order oligomers of *Bs*-ClpP, particularly heptamers and tetradecamers.

Observation of *Bs*-ClpP Alone and ADEP1 Mixture by HS-AFM. We utilized high-speed atomic force microscopy (HS-AFM) to confirm the ADEP1-induced oligomer formation of *Bs*-ClpP. Samples of *Bs*-ClpP (2.7 μM) alone and a mixture of *Bs*-ClpP and ADEP1 (monomer molar ratio of *Bs*-ClpP:ADEP1 = 1:2) were deposited onto a mica substrate for 5 min incubation before HS- AFM observation (Figure 2). In

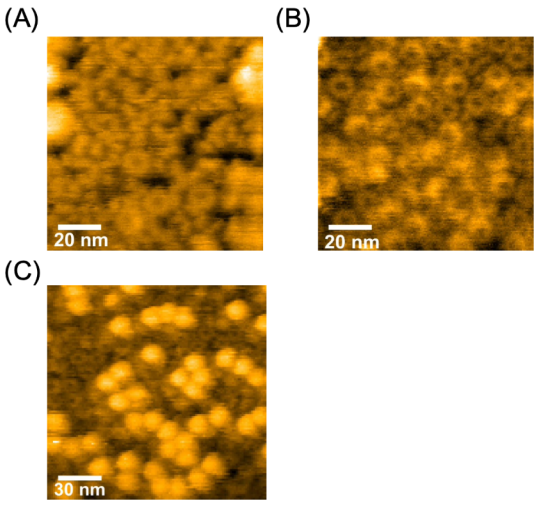

Figure 2. Observation of *Bs*-ClpP by HS-AFM. (A) HS-AFM images of *Bs*-ClpP and (B, C) a mixture of *Bs*-ClpP and ADEP1 at a molar ratio of ClpP:ADEP1 = 1:2.

the absence of ADEP1, *Bs*-ClpP exhibited ring structures along with numerous disjointed structures, suggesting incomplete ring formation, though the apo forms of ClpP from various species have been successfully crystallized in the tetradecameric state (PDB: 7feq, 8cj4, etc.). In contrast, when ADEP1 was added to *Bs*-ClpP, we observed tightly packed ring structures on the mica substrate with spherical structures overlapping the ring formations. To corroborate these results, we performed negative stain electron microscopy. Consistent with the HS-AFM observations, the addition of ADEP1 resulted in the formation of numerous ring structures (Figure 3). These results collectively demonstrate that ADEP1 promotes the assembly of *Bs*-ClpP into organized, higher-order structures, likely representing the heptameric and tetradecameric forms observed in native gel electrophoresis.

https://doi.org/10.1021/acsomega.4c11303
ACS Omega 2025, 10, 7381−7388

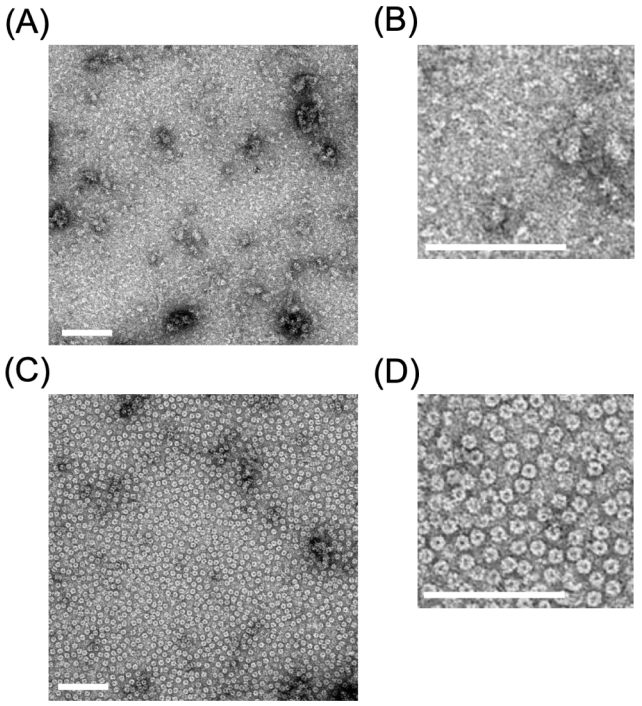

Figure 3. Negative-stain electron microscopy observation of *Bs*-ClpP. (A, B) Electron micrographs of *Bs*-ClpP alone. (C, D) Electron micrographs of a mixture of *Bs*-ClpP and ADEP1. Images (B) and (D) are partially enlarged portions of (A) and (C), respectively. White scale bars represent 100 nm.

To further characterize the structures observed via HS-AFM, we generated pseudo-AFM images based on the PDB data of *Bs*-ClpP (7FEP) of ClpP (Figure 4A).[20] The upper panel of Figure 4A displays pseudo-AFM images of the *Bs*-ClpP heptamer as viewed from the dimer interface, while the lower panel shows the opposite outward-facing surface. Comparing pseudo-AFM images with the actual HS-AFM observations shows striking similarities. The ring structures observed on the mica surface (Figure 4B) exhibited a central hole, consistent with the upper view of the heptameric pseudo-AFM image. The spherical structures stacked on top of these rings (Figure 4C) corresponded well with the lower view of the pseudo-AFM image. Height analysis of these structures (Figure 4D) showed that the spherical structures were approximately twice the height of the ring structure. Furthermore, ring structures were consistently observed beneath the spherical structures (Figure S4). Based on this evidence, we concluded that the ring structures observed by HS-AFM correspond to *Bs*-ClpP heptamers, while the spherical structures represent tetradecamers.

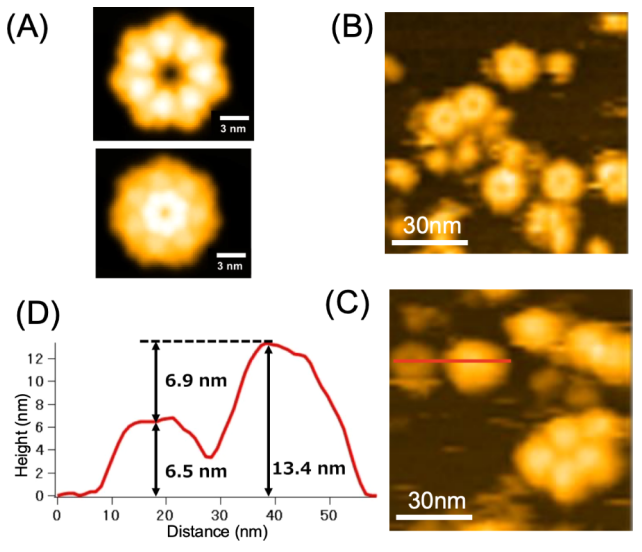

Figure 4. HS-AFM observation of ring structures composed of *Bs*-ClpP. (A) The pseudo-AFM images of *Bs*-ClpP heptamer are based on PDB: 7FEP. Upper images show the view from the bonding surface between heptamers, while lower images show the view from the opposite side. (B, C) Actual HS-AFM images of *Bs*-ClpP. The ADEP1 concentration was diluted 10-fold compared to the observation conditions in Figure 1, and the mixture contained 10% glycerol. (D) Cross-sectional profile along the red line in the image (C).

Process of *Bs*-ClpP Tetradecamer Formation. Our HS-AFM observations confirmed that ADEP1 promotes the formation of both heptameric rings and tetradecamers of *Bs*-ClpP. The prevalence of heptameric ring structures alongside tetradecamers suggests a sequential assembly process. We propose that tetradecamer formation proceeds through the following steps: initially, monomers or small oligomers assemble into heptameric rings (R state). Subsequently, these heptameric rings interact with each other to form double rings (2R state), ultimately resulting in the assembly of tetradecamers. However, it is important to note that while we have observed the end products of this assembly process, the dynamic transition from monomers to heptamers and from heptamers to tetradecamers has not been directly evidenced. These intermediate steps in the ADEP1-induced oligomerization of *Bs*-ClpP remain to be determined through real-time observation techniques. To gain further insights into these dynamic assembly processes, we aimed to capture the oligomerization of *Bs*-ClpP in real time by using HS-AFM.

Initially, *Bs*-ClpP (2.7 μM) was deposited onto a mica substrate and allowed to adsorb for 5 min before commencing HS-AFM observation. Subsequently, ADEP1 (32.7 μM) was added to the observation buffer, and observation continued. No immediate changes were observed in the initial field of view following ADEP1 addition. However, upon shifting the imaging area, we discovered numerous heptameric ring structures (Figure 5A). The image at t = 0 s in Figure 5A represents the state of *Bs*-ClpP immediately after the addition of ADEP1 in this new field of view. We acquired continuous HS-AFM images at an imaging speed of 1 s/frame, moving the imaging fields to capture different areas. However, direct observation of the assembly process from monomers to heptamers proved challenging. This difficulty likely arises from the small size of the ClpP monomer (diameter <5 nm), which makes it susceptible to physical disturbance by the probe tip during HS-AFM scanning. As a result, the assembly process may be significantly hindered during observation, making it difficult to capture the moment of ClpP monomer assembly using HS-AFM. Despite this limitation, we were able to observe the intermediate stages of the oligomerization process. Specifically, we captured images of *Bs*-ClpP, presumed to be in various oligomeric states, assembling to form a putative pentamer, which is observed in Figure 5B. Using time-lapse imaging at an imaging speed of 2 s/frame, we observed the process of monomers and dimers binding to form larger oligomers.

https://doi.org/10.1021/acsomega.4c11303
ACS Omega 2025, 10, 7381−7388

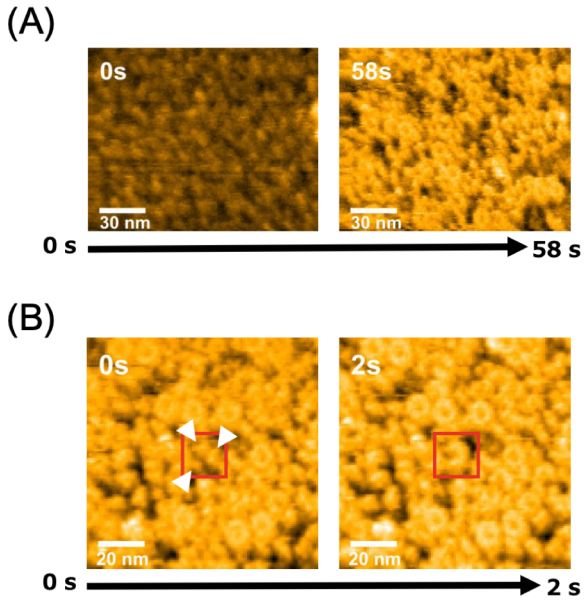

Figure 5. Process of *Bs*-ClpP heptamer formation. (A) HS-AFM observation of *Bs*-ClpP heptamer formation on a mica substrate upon the addition of ADEP1. Images were captured at a scanning speed of 1 s/frame. While new heptameric ring formations were not observed at the same location, they were detected upon moving the observation field. (B) HS-AFM images showing the assembly of *Bs*-ClpP monomers and dimers into oligomers. Images were captured at a scanning speed of 2 s/frame. The field containing the target molecules is indicated by a red frame. White arrows indicate monomers and dimers before binding. ADEP1 was added at a concentration of 32.7 μM.

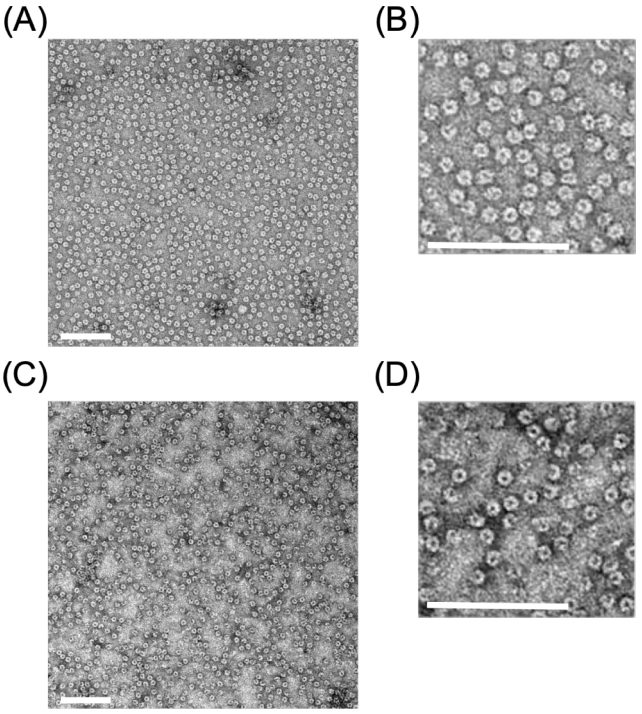

Figure 6. Negative-stain electron microscopy observation of *St*-ClpP. (A, B) Electron micrographs of *St*-ClpP alone. (C, D) Electron micrographs of a mixture of *St*-ClpP and ADEP1. Images (B) and (D) are partially enlarged portions of (A) and (C), respectively. White scale bars represent 100 nm.

Observation of *St*-ClpP by HS-AFM. To investigate whether the ADEP1-induced oligomerization observed in *Bs*-ClpP is a common feature among ClpP from different species, we purified and analyzed ClpP from *Salmonella enterica* serovar Typhimurium (*St*-ClpP). Unlike *Bs*-ClpP, which predominantly exists in non-ring structures in the absence of ADEP1, *St*-ClpP exhibited different behavior. We employed both HS-AFM and negative staining electron microscopy (EM) to characterize *St*-ClpP's oligomeric state. EM analysis revealed that *St*-ClpP readily formed ring structures even in the absence of ADEP1 (Figure 6A,B). Interestingly, the addition of ADEP1 did not significantly alter the observed structures; ring formations similar to those seen without ADEP1 were still prevalent (Figure 6C,D). Then we attempted to observe *St*-ClpP (56 μM) using HS-AFM under conditions similar to those used for *Bs*-ClpP (Figure 7). Initially, *St*-ClpP was deposited onto a bare mica substrate for 5 min before HS-AFM observation. However, *St*-ClpP demonstrated a markedly weak affinity for the bare mica surface. We observed few adsorbed molecules, and those present exhibited rapid diffusion across the substrate, making detailed HS-AFM imaging challenging. This behavior stands in stark contrast to that of *Bs*-ClpP, which readily adsorbed to bare mica surfaces. The distinct substrate interaction behaviors of *St*-ClpP and *Bs*-ClpP suggest significant differences in their surface charge characteristics. To address this issue, we modified our experimental protocol. The mica substrate was pretreated with (3-aminopropyl)triethoxysilane (APTES) for 5 min to alter its surface charges. *St*-ClpP was then applied to the modified substrate. This surface modification strategy significantly improved the adsorption and stability of *St*-ClpP molecules on the substrate, enabling more effective HS-AFM imaging.

Analysis of the HS-AFM profiles revealed that *St*-ClpP forms tetradecamers, even in the absence of ADEP1. Remarkably, the addition of ADEP1 did not induce significant changes in the observed structures. We carefully compared the size of the ring pores and the top structure of the tetradecamers in the presence and absence of ADEP1 but did not detect large structural changes. This observation contrasts with previous structural comparisons that reported an increase in ring size upon ADEP1 binding. Our HS-AFM observations failed to detect such a structural change in ring size. This discrepancy may be due to the resolution limits of HS-AFM or could suggest that the ADEP1-induced conformational changes in *St*-ClpP are more subtle than previously thought.

Interestingly, while the planar dimensions remained largely unchanged, we observed a difference in the height of the cross-sectional HS-AFM images. The tetradecamers without ADEP1 exhibited a height of approximately 6 nm, whereas those with ADEP1 showed an increased height of about 8 nm. This vertical expansion suggests that ADEP1 binding may induce a conformational change that primarily affects the axial dimensions of the *St*-ClpP complex.

DISCUSSION

The structural dynamics of ClpP in response to ADEP1 binding were previously investigated using various techniques. Cryo-EM studies of *Bs*-ClpP bound to ADEP1 revealed that ADEP1 activation induces a transition in the N-terminal segment gate of ClpP from a closed to an open state.[18,19] Notably, these conformational changes were primarily localized to the upper part of the ClpP complex. Recent

https://doi.org/10.1021/acsomega.4c11303
ACS Omega 2025, 10, 7381−7388

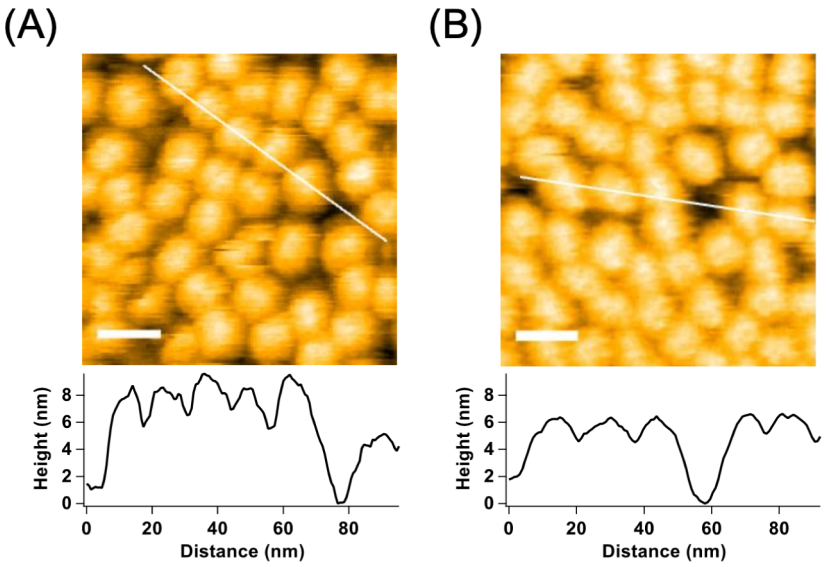

Figure 7. HS-AFM imaging of the *St*-ClpP ring structure. HS-AFM images of (A) *St*-ClpP alone, and (B) a mixture of *St*-ClpP and ADEP1. For both (A) and (B): Upper: HS-AFM images of *St*-ClpP on a mica substrate modified with 0.01% APTES. Lower: height profiles of the cross sections along the white lines in the upper images. White scale bars represent 20 nm.

advances in structural biology have further elucidated the conformational flexibility of *Bs*-ClpP. Crystal structure and cryo-EM analyses have demonstrated the existence of various conformational states under different pH conditions.[20] These findings underscore the remarkable structural plasticity of the ClpP complex.

In this study, we utilized HS-AFM to directly capture the behavior of the *Bs*-ClpP complex upon ADEP1 addition. This approach allowed us to visualize that the tetradecamer formation of *Bs*-ClpP consists of two distinct processes: the assembly of monomers into heptamers followed by the association of heptamers to form tetradecamers. Complementing our HS-AFM observations, native-gel electrophoresis analysis detected discrete bands corresponding to tetradecamer and heptamer states, with their relative abundances depending on ADEP1 concentration. Based on these findings, we propose a model for the ClpP assembly process induced by ADEP1, as illustrated in Figure 8. Unlike *Bs*-ClpP, ClpP derived from *Salmonella* (*St*-ClpP) forms tetradecameric ring structures without ADEP1, despite the high amino acid sequence homology between the two proteins. This difference in the basal oligomerization state highlights the species-specific variations in ClpP behavior. Interestingly, HS-AFM analysis revealed a significant structural change in *St*-ClpP upon ADEP1 addition. Contrary to what might be expected based on previous studies, the height of *St*-ClpP structures measured by HS-AFM decreased from approximately 8 nm in the absence of ADEP1 to about 6 nm in its presence. This observation is particularly intriguing, as it appears to contradict the extended conformation typically observed in side-view cryo-EM structures of ADEP1-bound ClpP.

Recent studies have provided new insights into the mechanism of ADEP action and ClpP regulation across different species. In *Streptomyces*, ADEP peptides have been shown to bind to the ClpP-ATPase site opposite the usual ClpP-ATPase binding site, promoting protease activity.[21] This suggests that ADEP may inhibit bacterial growth by disrupting the formation of heteromeric complexes involving ClpX, ClpC1, or ClpP2 with the ClpP1P2 core in the Clp protease

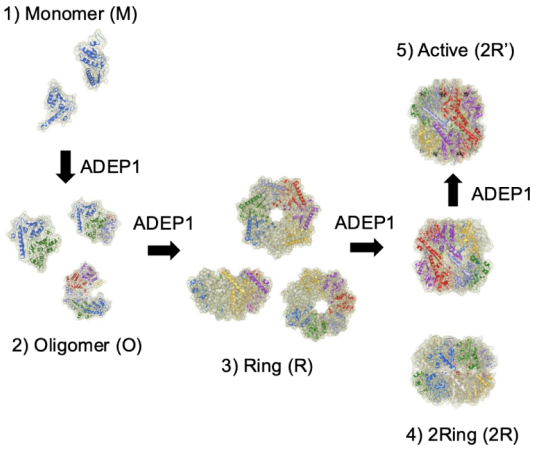

Figure 8. Proposed model of tetradecamer formation model of *Bs*-ClpP. The figure illustrates the stepwise assembly and activation process of *Bs*-ClpP. Initially, individual *Bs*-ClpP monomers (monomer state) interact to form small oligomers (Oligomer state). Stabilization of these interactions by factors such as glycerol or ADEP1 leads to the formation of heptameric rings (Ring state). Two heptameric rings then stack to form a tetradecamer (2Ring state). This 2Ring state is stabilized by glycerol or other substances but lacks protease activity against casein. Finally, ADEP1 binding to the 2Ring state activates the tetradecamer (Active state), conferring protease activity.

complex of *Streptomyces*. Structural studies of *Staphylococcus aureus* ClpP revealed conformational changes upon ADEP binding. The α5 helix transitions from a bent structure (PDB: 3QWD) to an extended structure (PDB: 6TTY).[22,23] In the tetradecameric state, the conformational changes lead to the formation of a hydrogen bond network between the two heptameric rings, as opposed to the loose contact observed in the compressed state.[23,24]

For *Bs*-ClpP, structural analysis has shown that ADEP1 binding involves hydrophobic amino acid residues, including Tyr112, Phe82, Leu48, and Tyr62.[15] ADEP1 activation causes a transition of the ClpP N-terminal segment from a closed to an open state, with conformational changes limited to the

https://doi.org/10.1021/acsomega.4c11303
ACS Omega 2025, 10, 7381−7388

upper part of ClpP. The hydrophobic amino acid cluster (Pro4, Val6, Tyr17, Ile19, Leu24, and Phe49) plays a crucial role in maintaining the N-terminal structure. Previous gel filtration studies have shown that *Bs*-ClpP oligomerization is influenced by both glycerol and ADEP1.[18] In the absence of glycerol, *Bs*-ClpP eluted as a monomer, while in the presence of 10% glycerol or ADEP1, it shifted to a tetradecameric state. Interestingly, the F49S of *Bs*-ClpP remained monomeric even in the presence of glycerol but formed a tetradecamer when exposed to ADEP1. These observations align with our HS-AFM findings for *Bs*-ClpP and *St*-ClpP. The structural changes induced by ADEP1 binding at the N-terminal site appear to promote ring formation through interactions with the surrounding structures. Moreover, these N-terminal structural changes seem to propagate to the C-terminal region, affecting the α5 helix. Our Native-PAGE results showed migration to positions consistent with heptamer and tetradecamer formations upon ADEP1 addition. However, gel filtration did not detect the heptameric state, possibly due to differences in experimental conditions.

The species-specific variations observed in our study, particularly the differences between *Bs*-ClpP and *St*-ClpP in their basal oligomerization states and responses to ADEP1, reflect the complex nature of ClpP regulation. While *Escherichia coli* ClpP (*Ec*-ClpP) has been reported to exist consistently as a tetradecamer, our observations of *Bs*-ClpP and *St*-ClpP reveal more dynamic oligomerization behaviors.

The antibacterial effect of ADEP1 is complex and is not universally effective across all bacterial species. Notably, bacteria can survive even when ClpP is deleted in *B. subtilis*[25] and several other species. This observation suggests that ADEP1 and its derivatives may not be suitable as broad-spectrum antibiotic drugs. The mechanism of ADEP1's antibacterial action is believed to be related to its promotion of protein degradation, potentially leading to the breakdown of essential proteins crucial for bacterial growth. One key protein identified in this context is FtsZ, which plays an essential role in cell division. Studies have shown that ADEP1 promotes the degradation of FtsZ, potentially contributing to its antibacterial effect.[26,27] This targeted degradation of essential proteins provides a possible explanation for ADEP1's growth-inhibitory effects in some bacterial species. In our study, we used casein as a model substrate to assess the protease activity of ClpP in the presence of ADEP1. While this approach provides valuable insights into the general proteolytic activity of ADEP1-activated ClpP, it may not fully capture the complexity of in vivo substrate degradation. To further elucidate the mechanism of ADEP1-induced protein degradation and its potential antibacterial effects, we propose to directly observe the degradation of physiologically relevant substrates such as FtsZ, as well as model substrates like casein, by ADEP1-activated ClpP using HS-AFM. This approach could allow us to visualize the degradation process in real-time and at the single-molecule level.

MATERIALS AND METHODS

Purification of ClpP. The *clpP* gene from *B. subtilis* was cloned into a pET21a expression vector, incorporating a C-terminal six-residue histidine affinity tag.[28] For protein expression and purification, the pET21a-*clpP* construct was transformed into *E. coli* BL21 (DE3) cells. An overnight culture of the transformed *E. coli* was inoculated into 2 L of LB medium supplemented with 100 μg/mL ampicillin. The culture was incubated at 37 °C with shaking until it reached an optical density (A_{600}) of 0.8. Protein expression was then induced by adding isopropyl β-D-1-thiogalactopyranoside (IPTG) to a final concentration of 0.5 mM. The culture was further incubated for 3 h at 37 °C. Cells were harvested by centrifugation and resuspended in lysis buffer (25 mM Tris-HCl, pH 7.5, 150 mM NaCl, 10% glycerol, 0.5% Triton X-100). Cell lysis was performed by sonication at 4 °C using an ultrasonic disruptor UD201 (Tomy Digital Biology Co., Ltd., Japan). The lysate was centrifuged to remove cell debris, and the supernatant was applied to a Ni Sepharose high-performance resin (GE Healthcare) for affinity chromatography. Bound proteins were eluted by using a linear gradient of imidazole (10−500 mM). Eluted fractions were analyzed by SDS-PAGE with Coomassie Brilliant Blue (CBB) staining. Protein concentrations were determined using the Bradford method. Fractions containing the recombinant ClpP were pooled and dialyzed against the assay buffer (25 mM Tris-HCl, pH 7.5, 150 mM NaCl, 10% glycerol).

Salmonella ClpP was obtained using the method described previously.[29]

Observation and Analysis of ClpP Protein Using High-Speed Atomic Force Microscopy (HS-AFM). HS-AFM observations were conducted at room temperature (approximately 25°C) using a buffer containing 25 mM Tris-HCl (pH 7.5) and 150 mM NaCl (25TN150). The cantilever's free vibration amplitude was set between 2 and 4 nm, with feedback control maintaining the amplitude at 60 to 90% of the free vibration amplitude.

Bs-ClpP was directly adsorbed onto a freshly cleaved mica substrate (Furuuchi Chemical Co., Ltd.), while *St*-ClpP was adsorbed onto a mica substrate modified with 3-aminopropyltriethoxysilane (APTES) to create a positively charged surface. Cylindrical glass stages (1.5 mm diameter, 2 mm height; Japan Cell Co., Ltd.) were used to mount the mica substrates. For APTES modification, 2 μL of 0.01% APTES solution was applied to the mica surface and incubated for 3 min, followed by washing with 60 μL of water. For sample application, 2 μL of appropriately diluted protein sample in 25TN150 buffer was applied to the prepared substrate and incubated at room temperature for 5 min. HS-AFM observations were performed in a total volume of 85 μL of 25TN150 buffer. ADEP1 and its derivatives, dissolved in DMSO, were mixed into the ClpP solution prior to the HS-AFM observation.

Pseudo-AFM images were created by simulating the collision between a conical probe and three-dimensional protein structure models. The structures used were Bs-ClpP heptamer (PDB: 7FEP),[17] *E. coli*-derived ClpP tetradecamer (PDB: 1YG6),[12] and *E. coli*-derived ClpP tetradecamer with ADEP1 (PDB: 3MT6).[11]

Oligomer Formation Detected by Native-PAGE. *Bs*-ClpP was prepared at a concentration of 11.5 μM in 25TN150 buffer (25 mM Tris-HCl, pH 7.5, 150 mM NaCl). ADEP1 was added to the ClpP solution at varying concentrations: 0 μM, 29 μM, 57.5 μM, or 115 μM. The mixtures were incubated at room temperature for 10 min. Following incubation, sample buffer (100 mM Tris-HCl, pH 7.0, 25% glycerol, and 0.005% bromophenol blue) was added at a ratio of 1:5 (v/v) to the protein samples. The prepared samples were then loaded onto a 5−20% gradient Native-PAGE gel (ATTO Corporation). Electrophoresis was carried out under non-denaturing

https://doi.org/10.1021/acsomega.4c11303
ACS Omega 2025, 10, 7381−7388

conditions to preserve the native oligomeric states of the proteins.

Casein Degradation Assay. The reaction mixture contained *Bs*-ClpP at 0.5 μM, β-casein (Sigma-Aldrich, C6905) at 15 μM, and ADEP1 (Cyman Chemical, 15305) at 0.88 μM. These components were combined in a buffer containing 20 mM Tris-HCl (pH 8.0), 1 mM TCEP, and 1 mM $MgCl_2$. The total reaction volume was not specified but can be adjusted as needed. The reaction mixture was incubated at 37 °C for 2 h. As a negative control, an equivalent volume of DMSO (the solvent for ADEP1) was added instead of the ADEP1 solution. Following incubation, the degradation of β-casein was analyzed by SDS-PAGE using a 5−20% gradient gel (ATTO Corporation). This gradient gel allows for optimal separation and visualization of both intact β-casein and its degradation products.

■ ASSOCIATED CONTENT

Supporting Information

The Supporting Information is available free of charge at https://pubs.acs.org/doi/10.1021/acsomega.4c11303.

Sequence alignment of ClpP proteins, structures of ClpP proteins, ClpP purification, and time-lapse HS-AFM (PDF)

Accession Codes

Bacillus subtilis subsp. subtilis str. 168 ClpP: WOA98459.1; *Salmonella enterica* serovar Typhimurium ClpP: UTL67090.1.

■ AUTHOR INFORMATION

Corresponding Authors

Fumihiro Ishikawa − *Faculty of Pharmacy, Kindai University, Higashi-osaka, Osaka 577-8502, Japan;* orcid.org/0000-0002-8681-9396; Email: ishikawa@phar.kindai.ac.jp

Genzoh Tanabe − *Faculty of Pharmacy, Kindai University, Higashi-osaka, Osaka 577-8502, Japan;* orcid.org/0000-0002-7954-8874; Email: g-tanabe@phar.kindai.ac.jp

Takayuki Uchihashi − *Division of Material Science, Graduate School of Science, Nagoya University, Nagoya 464-8602, Japan;* orcid.org/0000-0002-0263-5312; Email: uchihast@d.phys.nagoya-u.ac.jp

Authors

Kanji Takahashi − *Division of Material Science, Graduate School of Science, Nagoya University, Nagoya 464-8602, Japan*

Akiko Takaya − *Graduate School of Pharmaceutical Sciences, Chiba University, Chuo-ku, Chiba 260-8675, Japan; Medical Mycology Research Center, Chiba University, Chuo-ku, Chiba 260-8673, Japan*

Michio Homma − *Division of Material Science, Graduate School of Science, Nagoya University, Nagoya 464-8602, Japan; Department of Biomolecular Engineering, Graduate School of Engineering, Nagoya University, Nagoya 464-8603, Japan*

Complete contact information is available at: https://pubs.acs.org/10.1021/acsomega.4c11303

Author Contributions

#F.I. and K.T. contributed equally to this work. K.T., F.I., T.U., and M.H. designed the study; K.T., F.I., T.U., A.T., and M.H. performed the experiments; K.T., F.I., T.U., G.T., and M.H. analyzed the data; K.T. and M.H. wrote the manuscript.

Notes

The authors declare no competing financial interest.

■ ACKNOWLEDGMENTS

We thank Dr. Robert Kurzbauer and Prof. Tim Clausen at the Research Institute of Molecular Pathology (IMP) for providing the plasmid and Dr. Kimika Maki for the technical support in electron microscopy. This study was partially supported by JSPS KAKENHI Grant Number 24K01309 (to T.U.). This work was also supported by the Uehara Memorial Foundation (to F.I.), the Japan Foundation for Applied Enzymology (2023 and 2024), the Research Foundation for Pharmaceutical Sciences (to F.I.), Kindai University Research Enhancement Grants (IP004 and IP003) (to F.I.), and AMED-CREST Grant (JP23gm161004 and JP24gm161004) (to A.T.). Finally, we are grateful for the financial support provided by the Antiaging Project for Private Universities.

■ REFERENCES

(1) Olivares, A. O.; Baker, T. A.; Sauer, R. T. Mechanical protein unfolding and degradation. *Annu. Rev. Physiol.* **2018**, *80*, 413−429.

(2) Sauer, R. T.; Baker, T. A. AAA+ proteases: ATP-fueled machines of protein destruction. *Annu. Rev. Biochem.* **2011**, *80*, 587−612.

(3) Jastrab, J. B.; Darwin, K. H. Bacterial proteasomes. *Annu. Rev. Microbiol.* **2015**, *69*, 109−127.

(4) Ishikawa, F.; Homma, M.; Tanabe, G.; Uchihashi, T. Protein degradation by a component of the chaperonin-linked protease ClpP. *Genes Cells* **2024**, *29* (9), 695−709.

(5) Thompson, M. W.; Singh, S. K.; Maurizi, M. R. Processive degradation of proteins by the ATP-dependent Clp protease from *Escherichia coli*. requirement for the multiple array of active sites in ClpP but not ATP hydrolysis. *J. Biol. Chem.* **1994**, *269* (27), 18209−18215.

(6) Baker, T. A.; Sauer, R. T. ClpXP, an ATP-powered unfolding and protein-degradation machine. *Biochim. Biophys. Acta, Protein Struct. Mol. Enzymol.* **2012**, *1823* (1), 15−28.

(7) Brötz-Oesterhelt, H.; Beyer, D.; Kroll, H.-P.; Endermann, R.; Ladel, C.; Schroeder, W.; Hinzen, B.; Raddatz, S.; Paulsen, H.; Henninger, K.; Bandow, J. E.; Sahl, H.-G.; Labischinski, H. Dysregulation of bacterial proteolytic machinery by a new class of antibiotics. *Nat. Med.* **2005**, *11* (10), 1082−1087.

(8) Brötz-Oesterhelt, H.; Vorbach, A. Reprogramming of the caseinolytic protease by ADEP antibiotics: Molecular mechanism, cellular consequences, therapeutic potential. *Front. Mol. Biosci.* **2021**, *8*, 690902.

(9) Mabanglo, M. F.; Bhandari, V.; Houry, W. A. Substrates and interactors of the ClpP protease in the mitochondria. *Curr. Opin. Chem. Biol.* **2022**, *66*, 102078.

(10) Mabanglo, M. F.; Wong, K. S.; Barghash, M. M.; Leung, E.; Chuang, S. H. W.; Ardalan, A.; Majaesic, E. M.; Wong, C. J.; Zhang, S.; Lang, H.; Karanewsky, D. S.; Iwanowicz, A. A.; Graves, L. M.; Iwanowicz, E. J.; Gingras, A.-C.; Houry, W. A. Potent ClpP agonists with anticancer properties bind with improved structural complementarity and alter the mitochondrial N-terminome. *Structure* **2023**, *31* (2), 185−200.

(11) Li, D. H. S.; Chung, Y. S.; Gloyd, M.; Joseph, E.; Ghirlando, R.; Wright, G. D.; Cheng, Y.-Q.; Maurizi, M. R.; Guarné, A.; Ortega, J. Acyldepsipeptide antibiotics induce the formation of a structured axial channel in ClpP: A model for the ClpX/ClpA-bound state of ClpP. *Chem. Biol.* **2010**, *17* (9), 959−969.

(12) Bewley, M. C.; Graziano, V.; Griffin, K.; Flanagan, J. M. The asymmetry in the mature amino-terminus of ClpP facilitates a local symmetry match in ClpAP and ClpXP complexes. *J. Struct. Biol.* **2006**, *153* (2), 113−128.

(13) Kahne, S. C.; Darwin, K. H. Structural determinants of regulated proteolysis in pathogenic bacteria by ClpP and the proteasome. *Curr. Opin. Struct. Biol.* **2021**, *67*, 120−126.

(14) Malik, I. T.; Brötz-Oesterhelt, H. Conformational control of the bacterial Clp protease by natural product antibiotics. *Nat. Prod. Rep.* **2017**, *34* (7), 815−831.
(15) Ye, F.; Zhang, J.; Liu, H.; Hilgenfeld, R.; Zhang, R.; Kong, X.; Li, L.; Lu, J.; Zhang, X.; Li, D. Helix unfolding/refolding characterizes the functional dynamics of *Staphylococcus aureus* Clp protease. *J. Biol. Chem.* **2013**, *288* (24), 17643−17653.
(16) Alves França, B.; Falke, S.; Rohde, H.; Betzel, C. Molecular insights into the dynamic modulation of bacterial ClpP function and oligomerization by peptidomimetic boronate compounds. *Sci. Rep.* **2024**, *14* (1), 2572.
(17) Kirstein, J.; Hoffmann, A.; Lilie, H.; Schmidt, R.; Rübsamen-Waigmann, H.; Brötz-Oesterhelt, H.; Mogk, A.; Turgay, K. The antibiotic ADEP reprogrammes ClpP, switching it from a regulated to an uncontrolled protease. *EMBO Mol. Med.* **2009**, *1* (1), 37−49.
(18) Lee, B.-G.; Park, E. Y.; Lee, K.-E.; Jeon, H.; Sung, K. H.; Paulsen, H.; Rübsamen-Schaeff, H.; Brötz-Oesterhelt, H.; Song, H. K. Structures of ClpP in complex with acyldepsipeptide antibiotics reveal its activation mechanism. *Nat. Struct. Mol. Biol.* **2010**, *17* (4), 471−478.
(19) Kim, L.; Lee, B.-G.; Kim, M.; Kim, M. K.; Kwon, D. H.; Kim, H.; Brötz-Oesterhelt, H.; Roh, S.-H.; Song, H. K. Structural insights into ClpP protease side exit pore-opening by a pH drop coupled with substrate hydrolysis. *Embo J.* **2022**, *41* (13), No. e109755.
(20) Lee, B.-G.; Kim, M. K.; Song, H. K. Structural insights into the conformational diversity of ClpP from *Bacillus subtilis*. *Mol. Cells* **2011**, *32* (6), 589−595.
(21) Reinhardt, L.; Thomy, D.; Lakemeyer, M.; Westermann, L. M.; Ortega, J.; Sieber, S. A.; Sass, P.; Brötz-Oesterhelt, H.; Wright, G. D. Antibiotic acyldepsipeptides stimulate the *Streptomyces* Clp-ATPase/ClpP complex for accelerated proteolysis. *mBio* **2022**, *13* (6), No. e0141322.
(22) Geiger, S. R.; Böttcher, T.; Sieber, S. A.; Cramer, P. A conformational switch underlies ClpP protease function. *Angew. Chem. Int. Ed.* **2011**, *50* (25), 5749−5752.
(23) Malik, I. T.; Pereira, R.; Vielberg, M.-T.; Mayer, C.; Straetener, J.; Thomy, D.; Famulla, K.; Castro, H.; Sass, P.; Groll, M.; Brötz-Oesterhelt, H. Functional characterisation of ClpP mutations conferring resistance to acyldepsipeptide antibiotics in *Firmicutes*. *ChemBiochem* **2020**, *21* (14), 1997−2012.
(24) Ye, F.; Zhang, J.; Liu, H.; Hilgenfeld, R.; Zhang, R.; Kong, X.; Li, L.; Lu, J.; Zhang, X.; Li, D.; Jiang, H.; Yang, C.-G.; Luo, C. Helix unfolding/refolding characterizes the functional dynamics of *Staphylococcus aureus* Clp protease. *J. Biol. Chem.* **2013**, *288* (24), 17643−17653.
(25) Msadek, T.; Dartois, V.; Kunst, F.; Herbaud, M. L.; Denizot, F.; Rapoport, G. ClpP of *Bacillus subtilis* is required for competence development, motility, degradative enzyme synthesis, growth at high temperature and sporulation. *Mol. Microbiol.* **1998**, *27* (5), 899−914.
(26) Silber, N.; Pan, S.; Schäkermann, S.; Mayer, C.; Brötz-Oesterhelt, H.; Sass, P.; Søgaard-Andersen, L. Cell division protein FtsZ is unfolded for N-terminal degradation by antibiotic-activated ClpP. *mBio* **2020**, *11* (3), No. e01006−20.
(27) Sass, P.; Josten, M.; Famulla, K.; Schiffer, G.; Sahl, H.-G.; Hamoen, L.; Brötz-Oesterhelt, H. Antibiotic acyldepsipeptides activate ClpP peptidase to degrade the cell division protein FtsZ. *Proc. Natl. Acad. Sci. U.S.A.* **2011**, *108* (42), 17474−17479.
(28) Trentini, D. B.; Suskiewicz, M. J.; Heuck, A.; Kurzbauer, R.; Deszcz, L.; Mechtler, K.; Clausen, T. Arginine phosphorylation marks proteins for degradation by a Clp protease. *Nature* **2016**, *539* (7627), 48−53.
(29) Sato, Y.; Takaya, A.; Mouslim, C.; Hughes, K. T.; Yamamoto, T. FliT selectively enhances proteolysis of FlhC subunit in FlhD4C2 complex by an ATP-dependent protease, ClpXP. *J. Biol. Chem.* **2014**, *289* (47), 33001−33011.

https://doi.org/10.1021/acsomega.4c11303
ACS Omega 2025, 10, 7381−7388